Matthis Hofmann*, Dominik Fromme, Jörg Thiem, and Puian Tadayon

Intuitive Control of a Robotic Arm via Inertial Sensors and EMG for Assistive Applications

https://doi.org/10.1515/cdbme-2025-0226

Abstract: We present an intuitive, real-time control system for a 6-axis robotic arm, designed to support assistive applications in biomedical contexts. Using four MARG-based inertial sensors placed on the arm and hand, human motion is captured and mapped to robot kinematics via quaternion-based sensor fusion and a two-step calibration process. The resulting end-effector pose is scaled to match the robot's workspace, while EMG signals enable control of a robotic gripper through thumb-index gripping gestures.

The system enables direct, gesture-based control without extensive training, making it accessible for users with limited mobility but preserved upper limb function. Evaluation results confirm stable, low-latency operation during pick-and-place tasks, with users intuitively compensating for minor sensor inaccuracies through visual feedback. This approach demonstrates strong potential for assistive robotics in home or care environments, particularly where conventional control methods are unsuitable.

Keywords: Arm Robotic, Sensor Fusion, Remote Control

1 Introduction

Independence in daily life is crucial for people with mobility impairments, such as those resulting from spinal cord injuries or neurological conditions. Even with preserved upper limb function, tasks involving reach, dexterity, or environmental interaction can be difficult, especially in home or care settings without constant assistance [11]. Advances in computation, sensor integration, and additive manufacturing have boosted the development of intuitive human-robot interfaces [6]. Conventional control methods like joysticks or buttons require training [8] and often lack precision for fine tasks. MARG-based inertial sensing offers a natural alternative by mapping human arm motion to robot control. Earlier work either used three IMUs without capturing shoulder motion [5, 9], or four IMUs with complex inverse kinematics for non-anthropomorphic arms [1]. In this paper, we present

Dominik Fromme, Jörg Thiem , Puian Tadayon , University of Applied Sciences and Arts Dortmund, Dortmund, Germany

a novel, easy-to-implement end-to-end method for intuitive robot control, optimized for pick-and-place tasks. Our approach leverages computationally efficient quaternion-based orientation estimation, combined with a two-step calibration process mapping sensor data to endeffector pose. Through appropriate scaling, we fully utilize the robot's workspace while considering its physical constraints. Notably, our approach explicitly incorporates shoulder movements, thereby enhancing the naturalness and precision of the robotic control interface. Our method uses the following coordinate systems: Earth coordinates (E) (ENU convention), intermediate robot frame (irf), sensor coordinates (S_i) , and corresponding bodysegment frames (B_i) (figures 3 and 4).

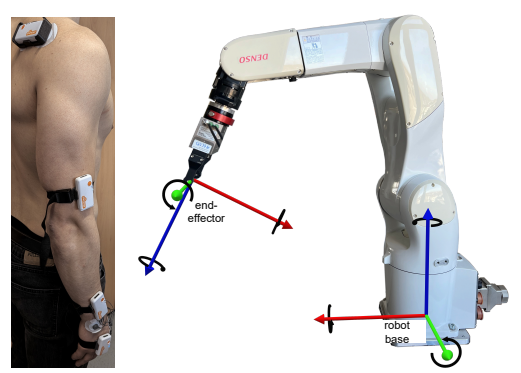


Fig. 1: Sensor Fig. 2: Denso VS-087 with attached WSG Gripper. Placement.

2 System Components

Motion data are captured using four Shimmer3 MARG sensors, placed at standardized anatomical positions to minimize soft-tissue artifacts, following Höglund et al. [3]. As shown in Figure 1, the sensors are mounted cranial-dorsally on the shoulder S_1 , and dorsally at the distal ends of the upper arm S_2 , forearm S_3 , and dorsally at the hand center S_4 . In addition, EMG signals from the Musculus interosseus dorsalis I are recorded to enable gripper control via muscle activity. After calibration, all sensors align with the coordinate system defined in Figure 3, using a consistent axis color scheme (X red, Y green, Z blue). The robotic platform is a 6-axis Denso VS-087 arm with a WSG-50-110 gripper, offering a reach of 1230.5 mm. Note that the end-effector coordinate frame is defined at the tip of the gripper, following safety conventions used in our lab.

497

^{*}Corresponding author: Matthis Hofmann, University of Applied Sciences and Arts Dortmund, Dortmund, Germany, e-mail: matthis.hofmann@fh-dortmund.de

3 Quaternion-based Sensor Fusion and Robot Control

3.1 Sensor Fusion and Calibration

To estimate segment orientations from inertial data, we apply a 9-DOF sensor fusion algorithm based on the Madgwick filter [12], chosen for its simplicity, speed, and reliable performance in dynamic environments. This algorithm fuses magnetometer, accelerometer, and gyroscope data, yielding real-time orientation estimates for each sensor, expressed as quaternions $\frac{S_i}{E}q$. Throughout this work, we use the notation $\frac{A}{B}q$ to denote the orientation of frame A relative to frame B, represented as a quaternion.

To ensure accurate and intuitive robot control, two calibration steps are performed: (1) determining the relative orientation between the intermediate robot and Earth frames $_{irf}^{E}q$, and (2) computing the relative alignment between each sensor and its corresponding body segment $_{S_i}^{B_i}q$, accounting for soft-tissue artifacts and sensor misplacement. Each segment orientation in the intermediate robot frame is then computed as:

3.1.1 Earth-to-Robot Calibration

The initial robot-to-earth orientation is derived from the shoulder orientation determined immediately prior to the start of motion capture. The default shoulder orientation in the intermediate robot frame is defined as ${B_1\over irf}q=\left[\frac{1}{2}\quad\frac{1}{2}\quad\frac{1}{2}\quad\frac{1}{2}\right],$ aligning the person's shoulder along the robot's negative Y-axis, with the positive X-axis pointing forward . Thus, hand movements in front of the user yield positive X-values (figure 4). As both Earth and robot frames share the same vertical (Z) axis, only a rotation around this axis, i.e. a yaw alignment, is required. Assuming identical yaw orientations (ψ) for the shoulder sensor and segment in the intermediate robot frame $({B_1\over irf}q_\psi={S_1\over irf}q_\psi)$, the orientation is computed as:

$$\psi_{E,irf} = \psi \begin{pmatrix} B_1 \\ irf \end{pmatrix} q \otimes S_1 \\ q^* \end{pmatrix}$$
 (2)

$$\frac{E}{irf}q = \left[\cos\left(\frac{\psi_{E,irf}}{2}\right) \quad 0 \quad 0 \quad \sin\left(\frac{\psi_{E,irf}}{2}\right)\right] \quad (3)$$

where $\psi(q)$ denotes the yaw angle extracted from quaternion q.

The shoulder sensor orientation ${}^{S_1}_Eq$ is averaged over five seconds of MARG data processed by the Madgwick algorithm.

3.1.2 Sensor-to-Segment Calibration

Sensor-to-segment calibration is performed using two predefined static postures (Figure 3), each held for approximately five seconds, in which the relative body segment orientations are known (Table 1). Inspired by [14], we compute the intrinsic average orientation of each sensor-segment pair by averaging yaw and pitch angles across all postures, disregarding roll due to anatomical variability. The resulting sensor-to-segment quaternions $\frac{S_i}{B_i}q$ provide robust segment orientation estimations for robot control.

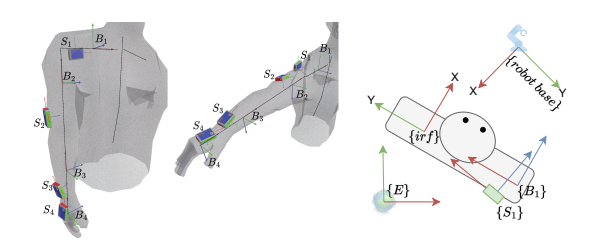


Fig. 3: Calibration postures A and B **Fig. 4:** Frame [2]. representations.

Algorithm 1 Sensor-to-segment calibration for calibration posture j (based on [4]).

```
1: Input: Sensor orientations: {}^{S_1}_{irf}q_j, {}^{S_2}_{irf}q_j, {}^{S_3}_{irf}q_j, {}^{S_4}_{irf}q_j, }
2: Body segment orientations: {}^{B_1}_{irf}q_j, {}^{B_2}_{B_2}q_j, {}^{B_3}_{B_2}q_j, {}^{B_4}_{B_3}q_j }
3: for i=2 to 4 do
4: {}^{B_i}_{irf}q_j \leftarrow {}^{B_{i-1}}_{irf}q_j \otimes {}^{B_i}_{B_{i-1}}q_j }
5: end for
6: for i=1 to 4 do
7: {}^{B_i}_{S_i}q_j \leftarrow {}^{S_i}_{irf}q_j^* \otimes {}^{B_i}_{irf}q_j 
8: {}^{B_i}_{S_i}q_j \leftarrow q_j(\psi({}^{B_i}_{S_i}q_j), \theta({}^{B_i}_{S_i}q_j), 0) \triangleright Yaw-Pitch only 9: end for
10: return {}^{B_1}_{S_1}q_j, {}^{B_2}_{S_2}q_j, {}^{B_3}_{S_3}q_j, {}^{B_4}_{S_4}q_j \triangleright Segment-to-sensor orientations
```

3.2 Segment Orientation Mapping to Intermediate Robot Frame

Segment orientations are mapped to the intermediate robot's coordinate frame using equation 1. Each segment is represented as a normalized vector with a total length of one aligned along the negative X-axis. Starting from the shoulder base p_0 , segment endpoints are computed sequentially, where each endpoint serves as the origin for the next segment. Vectors are rotated using the corresponding segment-to-irf quaternions, and final positions are determined as described in Algorithm 2

Tab. 1: Relative segment quaternions for sensor-to-segment calibration.

Posture	$\frac{irf}{B_1}q$	$_{B_{2}}^{B_{1}}q$	$^{B_2}_{B_3}q$	$\frac{B_3}{B_4}q$
Α	$\left[\frac{1}{2}, \frac{1}{2}, \frac{1}{2}, \frac{1}{2}\right]$	$\left[\frac{1}{2}, \frac{1}{2}, \frac{1}{2}, \frac{1}{2}\right]$	[1, 0, 0, 0]	[1, 0, 0, 0]
В	$\left[\frac{1}{2},\frac{1}{2},\frac{1}{2},\frac{1}{2}\right]$	$\left[\frac{1}{\sqrt{2}}, \frac{1}{\sqrt{2}}, 0, 0\right]$	[1, 0, 0, 0]	[1,0,0,0]

Algorithm 2 Conversion of Segment Orientation to Segment Positions.

- 1: **Input:** Body segment orientations: ${}^{B_1}_{irf}q$, ${}^{B_2}_{irf}q$, ${}^{B_3}_{irf}q$, ${}^{B_4}_{irf}q$ Normalized segment lengths: l_{B_1} , l_{B_2} , l_{B_3} , l_{B_4}
- 2: $p_{end,B_0} \leftarrow p_0 = \begin{bmatrix} 0 & 0 & 0 \end{bmatrix}$
- 3: **for** i = 1 to 4 **do**
- 4: $p_{end,B_i} \leftarrow p_{end,B_{i-1}} + rot_{vec} \begin{pmatrix} B_i \\ irfq, -l_{B_i} & 0 & 0 \end{pmatrix}$
- 5: end for
- 6: **return** p_{end,B_1} , p_{end,B_2} , p_{end,B_3} , $p_{end,B_4} >$ Segment positions

3.3 End-Effector Pose Adaptation

The estimated end-effector pose is passed to the robot controller, which computes the corresponding joint angles via inverse kinematics. To match the hand orientation with the robot's coordinate frame, the final segment quaternion $^{B_4}_{irf}q$ is rotated by -90° around the pitch axis.

To fit within the robot's constrained workspace, the position p_{end,B_4} is scaled by a factor r_2 and shifted by fixed offsets d_x and z_2 :

$$P_{irf} = P_{end,B_4} \cdot r_2 + \begin{bmatrix} d_x & 0 & z_2 \end{bmatrix} \tag{4}$$

We define two operating modes to constrain reachable regions and prevent collisions: (1) **full range** mode, allowing all positions in front of the shoulder (see Figure 5), and (2) **below shoulder** mode, which restricts movement to areas in front of and below the shoulder (see Figure 6). Depending on the application, a suitable mode can be selected, resulting in varying absolute movement changes of the robot for the same human arm movement.

3.4 Pose Validation and Filtering

Each estimated pose is first validated to ensure feasibility: the X-position must be positive, the Z-position above a minimum threshold z_{diff} , and the target must lie within the robot's reachable workspace.

To suppress jitter and involuntary fluctuations, e.g. due to muscle activation, pose updates are filtered using a delta-based method. Only if both Euclidean (position) and Riemannian (orientation) deviations from the previous pose exceed predefined thresholds, a new command is issued. This prevents unintended micro-movements and ensures smooth, stable robot motion.





Fig. 5: Full range [2].

Fig. 6: Below shoulder [2].



Fig. 7: Mirrored pick-and-place task.

3.5 EMG-Based Gripper Control

The gripper is controlled via EMG signals from the Musculus interosseus dorsalis I, which is responsible for thumb-index finger pinching. The raw signal is preprocessed using envelope detection and MVC normalization [7], enabling a consistent activation threshold across users.

A grasping action is triggered when the normalized EMG signal exceeds a threshold of 0.2 (relative to MVC) for at least 0.5 seconds. This trigger alternates the gripper between open and closed states. To avoid unintended activations, a hysteresis is applied: the signal must drop below the threshold for another 0.5 seconds before a new action can be triggered. This mechanism helps suppress short artifacts and ensures reliable, intentional control.

4 Evaluation

System performance was evaluated with respect to orientation accuracy, positional error and control latency. For ground-truth comparison, MARG sensor data were recorded simultaneously with a Vicon motion capture system during three motion types: slow and fast controlled movement, punctuated by short pauses at designated positions, and random movement. Resulting RMSE values and Euclidean distance errors along the kinematic chain are summarized in Table 2, showing increasing deviations with motion speed and distance from the base segment.

We also analyzed the impact of robot speed on latency and user experience. Due to mechanical limitations, execution time depends on joint acceleration constraints, axis limits, and speed settings. To determine the minimum speed required for intuitive robot control, we compared human and robot motion trajectories at various speed levels (see Table 3). When the robot was fast enough to mirror human motion fluidly, users could visually compensate for minor sensor inaccuracies, enabling reliable pick-and-place execution (see Figure 7).

Tab. 2: RMSE errors \bar{e} between and mean Euclidean distances \bar{d} between the Vicon and Shimmer orientations and points.

		cal slow	cal fast	random
	$S_1 q$	2.88	2.78	3.72
=(a)	S_2q	5.29	5.81	10.00
$\bar{e}(\circ)$	S_3q	2.88	2.83	4.53
	S_4q	5.19	6.08	5.16
	P_{end,B_1}	7.25	9.69	15.02
Ī(200 200)	P_{end,B_2}	21.07	28.85	60.93
d(mm)	P_{end,B_3}	28.35	31.08	62.15
	P_{end,B_4}	33.45	37.29	65.75
$\overline{d_{max}(mm)}$	P_{end,B_4}	103.22	88.96	162.16

Tab. 3: Fréchet distance [13] and normalized DTW [10] for different robot speeds.

Robot speed	100 %	50 %	30 %	10 %
Fréchet-Distance (mm)			17.036	40.333
normalized DTW (mm)	2.5595	4.878	7.265	18.537

5 Conclusion and Future Work

We presented an intuitive control interface for a 6-axis robotic arm, combining fused inertial sensing with EMG-based gripper actuation. The system enables natural, real-time control through arm gestures and thumb-index muscle activation, effectively supporting pick-and-place tasks within a human inthe-loop design. This allows for intuitive compensation of sensor noise through visual feedback, reducing the need for precise calibration. Unlike conventional interfaces, the system requires no extensive training, as users can control the robot through familiar, natural arm movements.

Evaluation results confirm sufficient spatial and temporal accuracy for practical use, as long as latency remains in tolerable range. The system shows strong potential as an assistive technology in biomedicine and rehabilitation. For individuals with limited mobility but preserved arm function, the telepresence robot system could enhance autonomy in daily life—particularly in home or care settings where continuous assistance is not available.

Future work will focus on optimizing latency, enhancing robustness under dynamic motion through trajectory path control, integrating camera-based feedback with predictive AI methods and validating the system in clinical or assistive environments to assess interindividual variability.

Author Statement

The authors declare no funding, no conflict of interest, and no ethical approval required.

References

- [1] Noccaro A, Cordella F, Zollo L, Di Pino G, Guglielmelli E, and Formica D. "A teleoperated control approach for anthropomorphic manipulator using magneto-inertial sensors." In: 2017 26th IEEE International Symposium on Robot and Human Interactive Communication (RO-MAN) (2017), pp. 156–161.
- [2] aaravanimates. Rigged Male Human 3D-Modell. 2025. URL: https://free3d.com/3d-model/rigged-male-human-442626.html (visited on 01/16/2025).
- [3] Höglund G, Grip H, and Öhberg F. "The importance of inertial measurement unit placement in assessing upper limb motion." In: Medical Engineering and Physics 92 (2021), pp. 1–9.
- [4] Vargas-Valencia LS, Elias A, Rocon E, Bastos-Filho T, and Frizera A. "An IMU-to-body alignment method applied to human gait analysis." In: Sensors (Basel) 16 (2016).
- [5] Kurpath MI, Bodireddy J Adwai P and, Chandrasekaran K, and Sam NK. "An IMUs and potentiometer-based controller for robotic arm-hand teleoperation." In: Sensors Actuators A Phys 367 (2024).
- [6] Corke P. Robotics, Vision and Control: Fundamental Algorithms In MATLAB®. 2nd ed. Cham: Springer International Publishing, 2017.
- [7] Konrad P. *EMG-FIBEL*: Eine praxisorientierte Einführung in die kinesiologische Elektromyographie. Velamed, 2011.
- [8] Tobias Rodehutskors, Max Schwarz, and Sven Behnke. "Intuitive bimanual telemanipulation under communication restrictions by immersive 3D visualization and motion tracking." In: 2015 IEEE-RAS 15th International Conference on Humanoid Robots (Humanoids) (2015), pp. 276–283.
- [9] Park S, Jung Y, and Bae J. "A tele-operation interface with a motion capture system and a haptic glove." In: 2016 13th Int Conf Ubiquitous Robots Ambient Intell (URAI) (2016), pp. 544–549.
- [10] Sakoe Hand Chiba S. "Dynamic programming algorithm optimization for spoken word recognition." In: *IEEE Trans* Acoust Speech Signal Process 26 (1978), pp. 43–49.
- [11] Kazuya Saita et al. "Feasibility of Robot-assisted Rehabilitation in Poststroke Recovery of Upper Limb Function Depending on the Severity." In: Neurologia medico-chirurgica (2020), pp. 217–222.
- [12] Madgwick SOH, Harrison AJL, and Vaidyanathan R. "Estimation of IMU and MARG orientation using a gradient descent algorithm." In: 2011 IEEE International Conference on Rehabilitation Robotics (2011), pp. 1–7.
- [13] Eiter T and Mannila H. Computing Discrete Fréchet Distance. CD-Laboratory for Expert Systems, TU Vienna, Austria, 1994.
- [14] Liu YT, Zhang YA, and Zeng M. "Sensor to segment calibration for magnetic and inertial sensor based motion capture systems." In: *Measurement* 142 (2019), pp. 1–9.